



<http://researchspace.auckland.ac.nz>

ResearchSpace@Auckland

Copyright Statement

The digital copy of this thesis is protected by the Copyright Act 1994 (New Zealand).

This thesis may be consulted by you, provided you comply with the provisions of the Act and the following conditions of use:

- Any use you make of these documents or images must be for research or private study purposes only, and you may not make them available to any other person.
- Authors control the copyright of their thesis. You will recognise the author's right to be identified as the author of this thesis, and due acknowledgement will be made to the author where appropriate.
- You will obtain the author's permission before publishing any material from their thesis.

To request permissions please use the Feedback form on our webpage.

<http://researchspace.auckland.ac.nz/feedback>

General copyright and disclaimer

In addition to the above conditions, authors give their consent for the digital copy of their work to be used subject to the conditions specified on the [Library Thesis Consent Form](#) and [Deposit Licence](#).

Note : Masters Theses

The digital copy of a masters thesis is as submitted for examination and contains no corrections. The print copy, usually available in the University Library, may contain corrections made by hand, which have been requested by the supervisor.

*New Concepts in Catalyst Design:
Homogeneous Organometallic Catalysts with
Tunable Architectures*

Kim Meyer Craig

*A thesis submitted in fulfillment of the requirements for the degree of Doctor of
Philosophy in Chemistry, The University of Auckland.*

Abstract

This thesis describes the development of homogeneous catalysts containing receptor elements which are capable of participating in reversible bonding interactions with groups bearing complementary functionality. This approach is amenable to combinatorial chemistry, and could facilitate catalyst development processes which are conventionally expensive and time-intensive. To date, the implications of reversible supramolecular interactions in anthropogenic organometallic catalysis are not widely understood.

Simplified pyridyl-borate ligands were prepared to simulate the behaviour of a larger target system composed of a 6,6'-boronic acid-2,2'-bipyridyl unit. Such a framework harnesses the power of reversible covalent bonding between boronic acids and diols. The reactivity of *ortho* and *meta*-pyridyl model ligands was investigated and knowledge gathered as to the hydrolytically unstable nature of the *ortho*-pyridyl borate moiety.

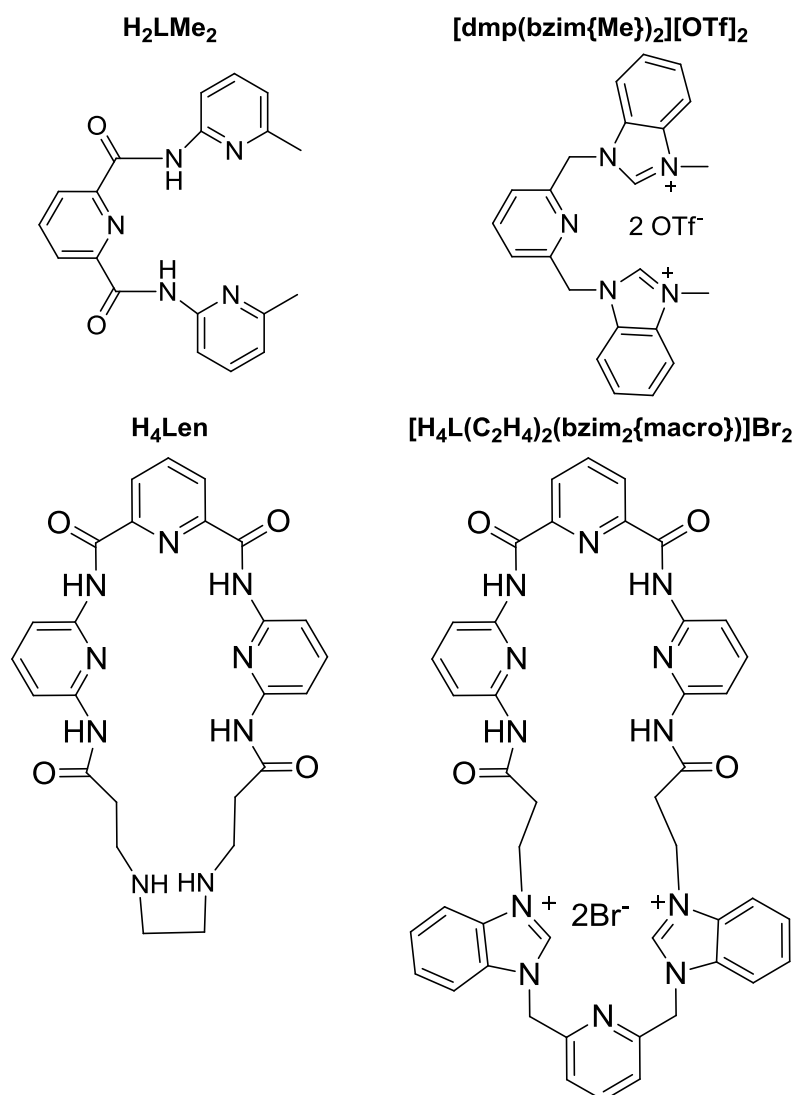
A macrocyclic ligand (**H₄Len**), formed via an aza-Michael ring-closing reaction between **N²,N⁶-bis(6-acrylamidopyridin-2-yl)pyridine-2,6-dicarboxamide** (**H₄LacrA**) and ethylenediamine was investigated as an appropriate framework for participation in supramolecular interactions. **N²,N⁶-bis(6-methylpyridin-2-yl)pyridine-2,6-dicarboxamide** (**H₂LMe₂**) was implemented as a model ligand with which to assess the head group ligating properties of the macrocyclic ring. Upon deprotonation of **H₂LMe₂** two amidate nitrogens are made available for binding to a metal centre. A series of novel iridium(III) and rhodium(III) complexes of **LMe₂** were prepared and tested for activity in the transfer hydrogenation of acetophenone using isopropanol. Appreciable activity was observed for **IrCl(py)₂(LMe₂)** and **IrCl₃(LMe₂{H}₂)** over the course of 24 hours, with 51 and 96% conversion of acetophenone into 1-phenylethanol respectively. By comparison, the macrocyclic complex, **(H₄Len)RuCl₂(MeCN)(PPh₃)₂**, mediated 38% conversion into 1-phenylethanol after 16.5 hours.

In pursuit of a second macrocyclic system bearing a bisbenzimidazolium tail, a simplified model ligand of **1,1'-(pyridine-2,6-diylbis(methylene))bis(3-methyl-1H-benzo[d]imidazol-3-ium) trifluoromethanesulfonate** (**[dmp(bzim{Me})₂][OTf]₂**) was prepared. Upon deprotonation with silver(I) oxide base a silver(I) MHC (*N*-heterocyclic carbene) was formed. This species was found to be an efficient intermediate by which palladium(II), rhodium(I) and iridium(I) dimethylpyridine bisbenzimidazol-2-ylidene complexes could be reached. Whilst providing a prelude to the target ligand, the rhodium(I) and iridium(I) MHCs were also found to be effective catalysts in the hydrosilylation of phenylacetylene using a range of silanes.

With the information gleaned from the model complex studies, the target ligand **[H₄L(C₂H₄)₂(bzim₂{macro})][Br]₂** was prepared via an aza-Michael ring-closing reaction between

H₄LacrA and **2,6-bis((1H-benzo[d]imidazol-1-yl)methyl)pyridine (dmp(bzim)₂)**). Subsequent mercuration of the ligand afforded two rare mercury(II) MHC complexes **[H₄L(C₂H₄)₂HgBr₂((MHC)₂{macro})]₂** and **[H₄L(C₂H₄)₂Hg((MHC)₂{macro})][HgBr₄]**, the latter of which was characterised by an X-ray diffraction study. Both of these materials demonstrated transmetalation to produce the macrocyclic pincer complex **[H₄L(C₂H₄)₂PdBr((MHC)₂{macro})][PF₆]**. Preliminary investigations were made into the activity of the macrocyclic palladium pincer MHC in the Heck-Mizoroki C-C coupling reaction between bromobenzene and styrene. While conversion into stilbenes after 24 hours was determined to be negligible with the macrocyclic complex alone, the inclusion of additives such as 2-amino-6-methyl pyridine dramatically increased substrate conversion to 84.2 (± 3.0)%. Subsequent analysis provided insight with regard to the nature of the active catalyst.

The novel ligand **[H₄L(C₂H₄)₂(bzim₂{macro})][Br]₂** and its MHC metal derivatives represent an innovative approach to homogeneous catalyst design which operates in proximity to receptor elements present within the macrocyclic ring.



Acknowledgments

I wish to thank A/P James Wright for his insights, assistance, support and patience during the course of my dissertation. Thanks also to Cees Lensink and Andy Falshaw who welcomed me to IRL Wellington and offered me a taste of industrial chemistry.

Many thanks go to the crystallographers who worked on my X-ray crystal structures, including Prof. George Clark, Assoc. Prof. Peter Boyd, Tania Groutso, Sen. Lect. Shane Telfer and Dr Christopher Fitchett.

Extensive gratitude is owed to the hardworking instrument and lab technicians at the University of Auckland. Michael Walker and Dr Michael Schmidt provided training and insight into the use of the NMR mass spectrometry facilities. Raisa Imatdieva has, more recently, functioned as the technician for mass spectrometry. Lab technicians, Joe Tizard and Radesh Singh, were invaluable and ensured the continuous operation of the laboratory.

Heartfelt thanks go to my dearest friend and colleague, Andrew Dalebrook - who was instrumental in solving and editing many tricky crystallographic problems that were encountered during the course of this dissertation. Your friendship has enriched this experience for me beyond measure.

Thanks to all my lab mates over the years, who provided a stimulating and friendly atmosphere in which to work, particularly, Laura, Paul, Lauren, J.D., Hayden, Dr Deborah Tonei and Folau. I specifically wish to thank Dr Michael Burgess, Dr Angela Slade and Dr Leon Lu for their friendly and professional guidance and support.

Financial assistance from the Bright Futures Top Achiever Doctoral Scholarship and the Chemistry Department of The University of Auckland, is gratefully acknowledged.

Most importantly, to my beloved husband Paul Craig – thank you for supporting me throughout this experience, for reading and editing my entire thesis and troubleshooting my technological difficulties. Thank you also, for knowing when to be empathic, when to be firm and when to supply coffee.

Table of Contents

Table of Contents

1	Chapter One: Introduction	1
1.1	Goals of the current work.....	2
1.2	General Introduction.....	2
1.3	Reversible Interactions: their application in nature and in synthesis.....	5
1.3.1	Activators or additives which direct catalysis	7
1.4	Applications for pyridyl borates	9
1.4.1	Suzuki C-C coupling reactions	9
1.4.2	1,2 and 1,3-diol receptors	10
1.5	Pincer Ligands with an NCN and NN'N binding motif	13
1.5.1	M(ECE) pincers	13
1.5.2	Phebox (M(NCN)) and Pybox (M(NNN)) pincers	16
1.5.3	M(N'NN') Pyridine Carboxamide pincers	18
1.5.4	2,6-pyridine carboxamide pincer ligands in supramolecular systems	20
1.6	<i>N</i> -Heterocyclic carbene ligands (MHCs) - Pincer Ligands with a CN'C binding motif.....	25
1.6.1	The electronic nature of carbenes	25
1.6.2	The electronic nature of free MHCs	26
1.6.3	The electronic nature of MHCs coordinated to transition metals.....	27
1.6.3.1	Thermochemistry – Bond Dissociation Energy (BDE) of the M-C _{NHC} bond...28	
1.6.3.2	Basicity of MHCs.....	29
1.6.3.3	Assessment of MHC electronic properties based upon trans CO substituted transition metals MHCs.....	30
1.6.4	Synthetic routes towards MHCs.....	31
1.6.5	Synthetic routes towards transition metal bearing MHCs.....	33
1.6.5.1	Preparation of silver(I) MHCs.....	33
1.6.6	MHCs in catalysis.....	37
1.6.6.1	Incorporating chirality into MHCs.....	38
1.6.7	Pincer MHCs.....	42
1.7	A comparison of pincer coordination pockets for binding to transition metals.....	44
1.8	Scope and outline of this thesis	46
2	Chapter Two: The design of pyridyl borate ligand systems for transition metals	47
2.1	Discussion.....	48
2.1.1	Project Aims	48
2.1.2	Model Complexes.....	49

2.1.2.1	[tris(3-pyridyl)boroxin].....	49
2.1.2.2	Preparation of 3-pyridylboronic acid esters of pinacol and catechol.....	50
2.1.2.3	Preparation of $\text{RuCl(Ph)(CO)(3-py-BO}_2\text{-C}_6\text{H}_{12}\text{)(PPh}_3\text{)}_2$	51
2.1.2.4	2-pyridyl boronic acids and esters.....	54
2.1.2.5	Hydrogenation of acetophenone using $\text{RuCl(Ph)(CO)(3-py-BO}_2\text{-C}_6\text{H}_{12}\text{)(PPh}_3\text{)}_2$	56
2.1.3	Preparation of the target complex	56
2.2	Conclusions.....	59
2.3	General Experimental.....	60
2.4	Experimental	60
3	Chapter Three: Novel acyclic and macrocyclic transition metal complexes composed of 2,6-pyridine carboxamide pincer ligands	64
3.1	Rhodium and Iridium complexes of H_2LMe_2	65
3.2	Preparation of $\text{MCl}_3(\text{LMe}_2\{\text{H}\}_2)$ (M = Rh/Ir)	65
3.3	Treatment of $\text{MCl}_3(\text{LMe}_2\{\text{H}\}_2)$ with base (M = Rh/Ir).....	71
3.3.1	Preparation of $\text{RhCl(py)}_2(\text{LMe}_2)$ (M = Rh/Ir) from pyridine base.....	71
3.3.2	Preparation of $\text{Rh(en)Cl(LMe}_2)$ and $[\text{Rh(en)}_2(\text{LMe}_2)]\text{[Cl]}$ from ethylenediamine.....	75
3.4	$[\text{RhCl}_2(\text{PPh}_3)(\text{LMe}_2\{\text{H}\}_2)]\text{[Cl]}$	80
3.4.1	Reactivity of $[\text{RhCl}_2(\text{PPh}_3)(\text{LMe}_2\{\text{H}\}_2)]\text{[Cl]}$ with various bases.....	84
3.4.1.1	Sodium Acetate yields Rhodium dimers of the type $[\text{RhX}(\text{LMe}_2)]_2$ (X = OAc/ Cl or OAc or Cl).....	84
3.5	Treatment of $\text{IrCl}_3(\text{LMe}_2\{\text{H}\}_2)$ with base	98
3.5.1	Preparation of $\text{IrCl(py)}_2(\text{LMe}_2)$ from pyridine base.....	98
3.5.2	Preparation of $[\text{IrCl}_3(\text{LMe}_2)]^{2-}$ by deprotonation of the pyridinium groups with strong base	102
3.5.3	Preparation of $\text{IrH(PPh}_3\text{)}_2(\text{LMe}_2)$ with potassium hydroxide, in the presence of triphenylphosphine	104
3.5.4	An imine analogue of $\text{LMe}_2 - \text{IrCl}_3(\text{L}_{\text{opy}}\{\text{Me}\}_2)$	108
3.6	Development of macrocyclic materials	113
3.6.1	$[(\text{H}_4\text{Len})\text{Rh(COD)}]\text{[Cl]}$	116
3.6.2	$[(\text{H}_4\text{Len})\text{RuCl(MeCN)(PPh}_3\text{)}_2]\text{Cl}$	117
3.7	Transfer Hydrogenation	121
3.7.1	Testing of rhodium(III) and iridium(III) complexes bearing acyclic and macrocyclic ligands derived from pyridine carboxamide building blocks.....	125
3.7.1.1	Results for transfer hydrogenation of acetophenone using isopropanol as a hydrogen source.....	126
3.8	Conclusions.....	132
3.9	Experimental	133
4	Chapter Four: Development of transition metal complexes bearing acyclic bisbenzimidazol-2-ylidenes.....	151
4.1	Development of transition metal complexes of the acyclic ligand $\text{dmp(NHC(Me)}_2\text{)}_2$	152
4.1.1	Preparation of acyclic $[\text{dmp(bzim}\{\text{Me}\}_2\text{)}_2]\text{X}_2$	152

4.1.2	Preparation of $[\text{Ag}(\text{dmp}(\text{NHC}(\text{Me})_2)_2)_2][\text{OTf}]_2$	156
4.1.3	Preparation and characterisation of palladium carbenes.....	158
4.1.3.1	Nitrile substituted analogues.....	158
4.1.3.2	Hydrolysis of acetonitrile coordinated to $[\text{Pd}(\text{dmp}(\text{NHC}(\text{Me})_2)_2)[\text{OTf}]_2$	160
4.1.3.3	Halide and cyano substituted analogues.....	168
4.1.4	Preparation of rhodium MHCs	172
4.1.4.1	$[\text{Rh}_2\text{Cl}_2(\text{COD})_2(\text{dmp}(\text{NHC}(\text{Me})_2)_2)]$	172
4.1.4.2	Carbonylation of $[\text{Rh}_2\text{Cl}_2(\text{COD})_2(\text{dmp}(\text{NHC}(\text{Me})_2)_2)]$	178
4.1.4.3	$[\text{Rh}_2(\mu\text{-CN})_2(\text{COD})_2(\text{dmp}(\text{NHC}(\text{Me})_2)_2)[\text{OTf}]$	182
4.1.5	Preparation of iridium carbenes.....	186
4.1.5.1	$[\text{Ir}(\text{COD})(\text{dmp}(\text{NHC}(\text{Me})_2)_2)[\text{OTf}]$	186
4.1.5.2	$[\text{Ir}_2(\mu\text{-CN})(\text{COD})_2(\text{dmp}(\text{NHC}(\text{Me})_2)_2)[\text{OTf}]$	194
4.1.5.3	Carbonylation product of $[\text{Ir}(\text{COD})(\text{dmp}(\text{NHC}(\text{Me})_2)_2)[\text{OTf}]$	196
4.1.6	The origins of CN^- in reaction mixtures of $[\text{dmp}(\text{NHC}(\text{Me})_2)_2][\text{OTf}]_2$ and Ag_2O	197
4.1.6.1	Alternative sources for cyanide: literature precedent for the generation of cyanide from azolium, transition metal NHCs and acetonitrile.....	200
4.2	Conclusions.....	203
4.3	Experimental	204
5	Chapter Five: Development of transition metal complexes bearing macrocyclic bisbenzimidazol-2-ylidenes.....	219
5.1	Development of macrocyclic ligands bearing bisbenzimidazoliums.....	220
5.1.1	Synthesis of $\text{H}_4\text{L}(\text{C}_2\text{H}_4)_2(\text{bzim})_2$	220
5.1.2	Synthesis of $\text{H}_4\text{L}(\text{C}_2\text{H}_4)_2(\text{imid})_2$	225
5.1.3	Synthesis of $[\text{H}_4\text{L}(\text{C}_2\text{H}_4)_2(\text{bzim}_2\{\text{macro}\})]\text{Br}_2$ and $[\text{H}_4\text{L}(\text{C}_2\text{H}_4)_2(\text{imid}_2\{\text{macro}\})][\text{Br}]_2$	227
5.2	Development of macrocyclic bisbenzimidazol-2-ylidene complexes of transition metals.....	231
5.2.1	Synthesis of $[\text{H}_4\text{L}(\text{C}_2\text{H}_4)_2\text{HgBr}_2((\text{NHC})_2\{\text{macro}\})]_2$ and $[\text{H}_4\text{L}(\text{C}_2\text{H}_4)_2\text{Hg}((\text{NHC})_2\{\text{macro}\})][\text{HgBr}_4]$	231
5.2.2	Preparation of the palladium macrocyclic NHC, $[\text{H}_4\text{L}(\text{C}_2\text{H}_4)_2\text{PdCl}((\text{NHC})_2\{\text{macro}\})][\text{PF}_6]$	242
5.3	Conclusions.....	255
5.4	Experimental	256
6	Chapter Six: <i>N</i> -Heterocyclic Carbenes in Catalysis.....	266
6.1	Hydrosilylation of alkynes promoted by homogeneous catalysis.....	267
6.1.1	Investigating the efficacy of newly synthesised <i>N</i> -Heterocyclic Carbenes rhodium(I) and iridium(I) catalysts in the hydrosilylation of phenylacetylene	271
6.1.1.1	Activity of the catalyst $\text{Rh}_2\text{Cl}_2(\text{COD})_2(\text{dmp}(\text{NHC}(\text{Me})_2)_2)$	275
6.1.1.2	Activity of the catalyst $[\text{Rh}_2(\mu\text{-CN})_2(\text{COD})_2(\text{dmp}(\text{NHC}(\text{Me})_2)_2)[\text{OTf}]$	279
6.1.1.3	Activity of the catalyst $[\text{Ir}_2(\mu\text{-CN})_2(\text{COD})_2(\text{dmp}(\text{NHC}(\text{Me})_2)_2)[\text{OTf}]$	282
6.1.1.4	Activity of the catalyst $[\text{Ir}(\text{COD})(\text{dmp}(\text{NHC}(\text{Me})_2)_2)[\text{OTf}]$	285
6.1.2	Summary	289

6.2	Heck-Mizoroki (C-C Coupling) Reactions	291
6.2.1	Activity of palladium NHCs in the Heck-Mizoroki reaction	295
6.2.1.1	Findings for acyclic pincer palladium benzimidazol-2-ylidenes.....	303
6.2.1.2	Findings for the macrocyclic pincer palladium benzimidazol-2-ylidene, [H ₄ L(C ₂ H ₄) ₂ PdBr((NHC) ₂ {macro})][PF ₆].....	306
6.2.1.3	C-C coupling reactions between ⁿ butyl acrylate and bromobenzene.....	314
6.2.1.4	Comparison to palladium pyridine carboxamide complexes.....	316
6.2.2	Summary	319
6.3	Experimental Procedures:.....	320
6.3.1	Hydrosilylation of phenylacetylene procedure.....	320
6.3.2	Heck-Mizoroki reaction procedures	320
6.3.3	Synthesis of a palladium(II)-amino methyl pyridine aggregate	322
7	Final Conclusions	323
8	Appendix - Synthetic Schemes	325
8.1	Schemes for Chapter Three.....	326
8.2	Schemes for Chapter Four.....	328
8.3	Schemes for Chapter Five	330

A compact disc containing the key files for all X-ray crystal structure determinations is enclosed within the jacket of this thesis.

List of Figures

Figure 1: Examples of 'privileged' ligands in metal catalysis	3
Figure 2: A comparison of combinatorial and iterative approaches to catalyst design	4
Figure 3: Reversible interactions within histidine and cytochrome c-reductase	5
Figure 4: Application of the DNA base-pair model to homogeneous catalyst design	6
Figure 5: Asymmetric hydrogenation using self-assembled phosphonite rhodium(I) catalysts	7
Figure 6: Enantioselective alkylation of benzaldehyde using activators in conjunction with zinc(II) diols	8
Figure 7: Mediation of (-)-sparteine in the palladium catalysed aerobic oxidative kinetic resolution of secondary alcohols.....	8
Figure 8: Examples of <i>o</i> and <i>m</i> -pyridyl boronic acids used in Suzuki cross-coupling reactions.....	9
Figure 9: Suzuki coupling reaction between 2-pyridinylboronate and 3,5-dimethyl-2-bromo-pyridine.	10
Figure 10: A chiral receptor for <i>D</i> -Fructose.....	10
Figure 11: Schematic for the covalent bonding association of diols with boronic acid and boronate ..	10
Figure 12: A PET boronic acid sensors for diol bindings.....	11
Figure 13: Ru (II) 5,6-dihydroxy-1,10-phenanthroline)]][PF ₆] ₂ as an indicator for reversible binding of glucose by a boronic acid.....	11
Figure 14: <i>N</i> -alkylation of 3-pyridylborate ribonucleoside receptors	12
Figure 15: 4,4'-diboronic-2,2'-bipyridine sugar receptors coupled with cobalt for chiroselective synthesis of Δ -[Co ^{III} (bpy) ₃] ²⁺	12
Figure 16: Attributes of the ECE ligand system	14
Figure 17: Techniques for metalation of ECE pincer systems.....	14
Figure 18: Functionalisation of ECE pincers towards practical applications	15
Figure 19: Transfer hydrogenation with a Ru(ECE) pincer.....	16
Figure 20: Transfer hydrogenation mediated by a terdentate Ru(II) Phebox complex.....	16
Figure 21: Typical procedure for the synthesis of pybox ligands	17
Figure 22: Hydrosilylation mediated by a terdentate Rh(II) pybox complex.....	17
Figure 23: The influence of phebox and pybox ligand systems on the rhodium coordination sphere .	17
Figure 24: The binding modes of carboxamides and pyridinamides.....	18
Figure 25: Binding modes of a pyridinamide ligand within the Trost allylic alkylation reaction.....	19
Figure 26: Transition metal complexes bearing 2,6-pyridine carboxamide bispyridinium ligands	19
Figure 27: U-shaped conformation of the 2,6-pyridine carboxamide moiety	20
Figure 28: 2,6-pyridine carboxamide ligands as hydrogen bonding receptors for anions and small molecules.....	21
Figure 29: A biomimetic host for the binding of adrenaline.....	21
Figure 30: The effect of metal templating upon ligand organisation	22
Figure 31: Janus-type molecular recognition exhibited by a copper(II) 2,2'-bipyridine 4,4'-diacylaminopyridine complex.....	23
Figure 32: Assembly of unique macrocyclic rings on a [3]rotaxane	23
Figure 33: Active palladium(II) [2]rotaxane template catalyst for the Heck C-C coupling reaction under base free conditions ⁵⁷	24
Figure 34: Spin Multiplicity of Singlet and Triplet Carbenes	25
Figure 35: The influence of frontier orbital energies upon the geometry of carbenes.....	26
Figure 36: Inductive effects of σ -electron withdrawing substituents and mesomeric effects of π -electron donating substituents upon a singlet state carbene.....	26
Figure 37: <i>MHC</i> π and π^* orbital interactions with metal d orbitals.....	27
Figure 38: Steric influence of substituted <i>MHCs</i> upon Bond Dissociation Energies of the Ru-C _{<i>MHC</i>} bond in a series of Cp [*] RuCl(<i>MHC</i>) complexes.....	29
Figure 39: pK _a ^{H₂O} (\pm) values for a series of <i>MHCs</i> , demonstrating <i>N</i> -substituent effects and the influence of substitution at the backbone	30
Figure 40: Synthetic routes towards the formation of <i>MHCs</i>	32
Figure 41: Methods for the formation of silver(I)- <i>MHCs</i>	34
Figure 42: Crystallographically observed structures for silver <i>MHCs</i>	35
Figure 43: Methods for the formation of transition metal bearing <i>MHCs</i>	36

Figure 44: Backbone and wingtip tuning of a free <i>N</i> -heterocyclic carbenes.....	38
Figure 45: Hydrogenation of arylalkenes using a chiral iridium MHC-oxazoline hybrid catalyst.....	39
Figure 46: Hydrogenation of a 1,1-disubstituted alkene.....	40
Figure 47: Rigid <i>N</i> -phenylcarbene bearing a stereogenic metal centre	40
Figure 48: Asymmetric ring-closing metathesis of a trialkene.....	40
Figure 49: Asymmetric hydrosilylation of ketones.....	41
Figure 50: Isomers of a Palladium di-triazolinylidene diiodide complex, differentiated by their axial chirality.....	41
Figure 51: Asymmetric hydrogenation of an alkene.....	42
Figure 52: Palladium(II) complexes analysed as catalysts in Suzuki coupling reactions.....	42
Figure 53: Literature examples of the transition metal CNC bisimidazol-2-ylidene pincers	43
Figure 54: Literature examples of cyclic polycarbenes.....	43
Figure 55: Bond length and angle characteristics of palladium pincers	44
Figure 56: Summarised representation of the characteristics of various pincer classes containing nitrogen and carbon atoms for coordination to palladium(II)	45
Figure 57: Key attributes of a 6,6'-boronic acid-2,2'-bipyridyl ligand system.....	48
Figure 58: Self assembly of combinatorial libraries built from a 6,6'-(B(O) ₂) ₂ -2,2'-bipy framework	48
Figure 59: Literature method for the preparation of 2-pyridylboronic acid ²²	49
Figure 60: Method for the synthetic preparation of [tris(3-pyridyl)boroxin] ¹⁰⁹	50
Figure 61: Preparation of 3-pyridylboronic acid esters from [tris(3-pyridyl)boroxin] ¹⁰⁹	50
Figure 62: Overlaid ¹ H NMR spectra for RuCl(CO)(Ph)(3-py-BO ₂ -C ₆ H ₁₂)(PPh ₃) ₂ and 3-py-BO ₂ -C ₆ H ₁₂	52
Figure 63: Expansion of the ¹³ C{ ¹ H} NMR (CDCl ₃ , ppm) spectrum for RuCl(CO)(Ph)(3-py-BO ₂ -C ₆ H ₁₂)(PPh ₃) ₂	53
Figure 64: Destabilisation of <i>ortho</i> -lithiated pyridines.....	54
Figure 65: Cross-coupling reactions between chloropyridines and tetra(pinacolato)boron.....	54
Figure 66: Literature methods for the stabilisation of 2-pyridyl boronic acids or esters	55
Figure 67: Preparation of dimethyl 2-pyridylboronate ²³	56
Figure 68: Synthetic procedure for 6,6'-Br ₂ -2,2'-bipy	56
Figure 69: Preparation of bipyridinediborate complexes from 6,6'-Br ₂ -2,2'-bipyridine	57
Figure 70: Preparation of (2,2'-bipyridine-6,6'-bisdiisopropoxydi(2-thienyl)borato)]-	57
Figure 71: H ₄ Len	64
Figure 72: Scheme for the formation of RhCl ₃ (LMe ₂ {H}) ₂ (M = Rh/Ir)	65
Figure 73: X-ray crystal structure for RhCl ₃ (LMe ₂ {H}) ₂ , R ₁ = 2.4%.....	67
Figure 74: Solid state characteristics of RhCl ₃ (LMe ₂ {H}) ₂	68
Figure 75: X-ray crystal structure for IrCl ₃ (LMe ₂ {H}) ₂ , R ₁ = 4.2%.....	69
Figure 76: Proposed mechanism for the pyridinium mediated reduction of nitrite	70
Figure 77: Fragmentation of RhCl(py) ₂ (LMe ₂) by ESI mass spectrometry	71
Figure 78: Selected bond lengths and angles for RhCl(py) ₂ (LMe ₂)	72
Figure 79: X-ray crystal structure of RhCl(py) ₂ (LMe ₂), R ₁ = 6.75%.....	73
Figure 80: NOESY ¹ H- ¹ H through space correlation experiment (600 ms) with RhCl(py) ₂ (LMe ₂) (CDCl ₃ , 300 MHz).....	74
Figure 81: ¹ H- ¹ H COSY spectrum of Rh(en)Cl(LMe ₂) demonstrating the ³ J _{HH} correlations between protons in the bidentate ethylenediamine substituent	76
Figure 82: ¹ H- ¹ H COSY spectrum of [Rh(en) ₂ (LMe ₂)]Cl demonstrating the ³ J _{HH} correlations between protons in the bidentate and monodentate ethylenediamine substituents	77
Figure 83: Expansion of the methylene and methyl regions for complexes Rh(en)Cl(LMe ₂) and [Rh(en) ₂ (LMe ₂)]Cl	77
Figure 84: X-ray crystal structure of Rh(en)Cl(LMe ₂), R ₁ = 9.75%.....	79
Figure 85: ³¹ P{ ¹ H} NMR (d ₆ -DMSO) spectrum of [RhCl ₂ (PPh ₃)(LMe ₂ {H}) ₂][Cl]	80
Figure 86: X-ray crystal structure for [RhCl ₂ (PPh ₃)(LMe ₂ {H}) ₂][Cl], R ₁ = 4.59%	83
Figure 87: Solid state intramolecular interactions and packing characteristics of [RhCl ₂ (PPh ₃)(LMe ₂ {H}) ₂][Cl] within the solid state.....	83
Figure 88: General procedure for the preparation of rhodium(III) dimeric complexes of LMe ₂ (Key - [RhCl(LMe ₂) ₂]: X ₁ = X ₂ = Cl; [Rh(OAc)(LMe ₂)] ₂ : X ₁ = OAc, X ₂ = Cl; [Rh(OAc)(LMe ₂) ₂]: X ₁ = X ₂ = OAc)	84
Figure 89: Right and left-handed isomers of [Pd(LMe ₂) ₂]	85
Figure 90: C ₂ rotational axis of [Rh(OAc)(LMe ₂) ₂]	85
Figure 91: ESI mass spectrum of [Rh(OAc)(LMe ₂) ₂], 880-1020 <i>m/z</i> mass range.....	87
Figure 92: ESI mass spectrum of [Rh(OAc)(LMe ₂) ₂], 447-453 <i>m/z</i> mass range.....	87

Figure 93: Simplified schematic for the formation of rhodium(III) LMe ₂ dimers	88
Figure 94: Expansion of the pyridyl region sourced from the ¹ H NMR spectrum of [RhCl(LMe ₂) ₂] (CDCl ₃ , ppm).....	89
Figure 95: Expansion of the quaternary carbon region for [RhCl(LMe ₂) ₂] (¹³ C{ ¹ H} NMR, CDCl ₃ , ppm)	89
Figure 96: Overlaid spectra featuring signals for the quaternary carbons of the three dimeric rhodium species.....	91
Figure 97: Three 4-membered rings presented in the X-ray crystal structure of [Rh(OAc)(LMe ₂) ₂]	92
Figure 98: X-ray crystal structure of [RhCl(LMe ₂) ₂], R ₁ = 4.4%.....	92
Figure 99: X-ray crystal structure of [Rh(OAc)(LMe ₂) ₂], R ₁ = 9.5%,.....	94
Figure 100: An example of μ ² , κ ³ coordination of an amide ligand to two rhodium centres	95
Figure 101: Aerobic oxidation of dihydrogen gas and alcohol using a dimeric Rh sulfonamido redox interconversion process	96
Figure 102: Carbonylation of [(Cp* ^{III} Rh) ₂ (μ-NTs) ₂]	97
Figure 103: Selected bond lengths and angles for rhodium complexes bearing amidate bridges	97
Figure 104: Expansion of the ¹ H- ¹ H COSY (CDCl ₃) spectrum for IrCl(py) ₂ (LMe ₂).....	98
Figure 105: Expansion of the ¹³ C{ ¹ H} NMR (CDCl ₃) pyridyl CH region for IrCl(py) ₂ (LMe ₂)	99
Figure 106: X-ray crystal structure of IrCl(py)(H ₂ O)(LMe ₂), R ₁ = 4.64%	100
Figure 107: Examples of Ir-aqua complexes	101
Figure 108: Solid state packing characteristics of IrCl(py)(H ₂ O)(LMe ₂)	101
Figure 109: ESI (positive mode) mass spectrum of [IrCl ₃ (LMe ₂)] ₂ [K] ₂	102
Figure 110: Overlaid ¹ H NMR (d ₆ -DMSO) spectra of IrCl ₃ (LMe ₂)(H) ₂ versus [IrCl ₃ (LMe ₂)] ₂ [K] ₂ , expansion of the pyridyl CH regions	103
Figure 111: Proposed mechanism for the formation of IrH(PPh ₃) ₂ (LMe ₂)	104
Figure 112: ¹ H NMR spectrum (400 MHz, CDCl ₃) of IrH(PPh ₃) ₂ (LMe ₂)	105
Figure 113: Expansion of the phenyl region in the ¹³ C{ ¹ H} NMR (CDCl ₃ , ppm) spectrum of IrH(PPh ₃) ₂ (LMe ₂)	106
Figure 114: X-ray crystal structure for IrH(PPh ₃) ₂ (LMe ₂), R ₁ = 4.57%	107
Figure 115: Coordination of an imine resonance form to iridium(III) trichloride	108
Figure 116: Metal imido complexes of palladium(II) and iridium(III).....	109
Figure 117: ¹ H- ¹³ C HMBC spectrum of IrCl ₃ (L _{opy} {Me}) ₂	111
Figure 118: ESI-MS(positive) spectrum of IrCl ₃ (L _{opy} {Me}) ₂	112
Figure 119: Scheme for the preparation of H ₄ Len and H ₄ L _n Bu, including a visual representation of the metal binding modes possible with these ligands ^{108,139}	114
Figure 120: The products of <i>aza</i> -Michael addition reactions between chiral diamines and H ₄ Lac ^r A	115
Figure 121: ¹ H NMR spectrum (d ₆ -DMSO) for [(H ₄ Len)Rh(COD)][Cl], indicating the downfield position of the diamine protons at δ 5.69 ppm	117
Figure 122: Expansion of the FAB mass spectrum for [(H ₄ Len)RuCl(MeCN)(PPh ₃) ₂] ₂ Cl	118
Figure 123: Expansion of the phenyl region in the ¹³ C{ ¹ H} NMR (CDCl ₃) spectrum for [(H ₄ Len)RuCl(MeCN)(PPh ₃) ₂] ₂ Cl.....	119
Figure 124: ¹³ C- ¹ H HSQC spectrum (CDCl ₃ , ethylene region) of [(H ₄ Len)RuCl(MeCN)(PPh ₃) ₂] ₂ Cl... ..	120
Figure 125: ¹ H- ¹ H COSY spectrum (CDCl ₃ , ethylene region) of [(H ₄ Len)RuCl(MeCN)(PPh ₃) ₂] ₂ Cl	120
Figure 126: Transfer hydrogenation (R ₁ ≠R ₂)	122
Figure 127: Diagrammatic representation of inner sphere transfer hydrogenation catalytic intermediates.....	122
Figure 128: Generic mechanism for the transfer hydrogenation of acetophenone using isopropanol as a hydrogen donor source (R ₁ = Ph, R ₂ = Me)	123
Figure 129: Transfer hydrogenation of methanol using Noyori's amine derived ruthenium(II) catalysts (Y = NTs).....	124
Figure 130: Hydrogenation mediated by alkoxide base in the presence of a hydrogen atmosphere ¹⁵⁴	126
Figure 131: Proposed mechanism for the transfer hydrogenation of acetophenone mediated by catalysts of the type IrHL ₂ (LMe ₂) (where L = PPh ₃ or pyridine)	129
Figure 132: Ruthenium(II) catalysts for transfer hydrogenation.....	130
Figure 133: Formation of a mixed amido-amine ligand from diamine and strong base	131
Figure 134: Proposed mechanism for the formation of a catalytically active Ru-H intermediate bearing a macrocyclic diamine ligand	131
Figure 135: The relative rates of conversion of acetophenone to 1-phenylethanol mediated by the catalysts IrCl(py) ₂ (LMe ₂), IrCl ₃ (LMe ₂)(H) ₂ and [(H ₄ Len)RuCl(MeCN)(PPh ₃) ₂] ₂ Cl.....	131

Figure 136: Schematic for the formation of dmpBr_2 , $\text{dmp}(\text{bzim})_2$ and $[\text{dmp}(\text{bzim}\{\text{Me}\})_2]\text{X}_2$	152
Figure 137: Crystal structure of $[\text{dmp}(\text{bzim}\{\text{Me}\})_2]_2$, $R_1 = 3.88\%$	154
Figure 138: Solid state crystal packing of $[\text{dmp}(\text{bzim}\{\text{Me}\})_2]_2$	154
Figure 139: ESI mass spectrum of $[\text{Ag}(\text{dmp}(\text{NHC}\{\text{Me}\})_2)_2][\text{OTf}]_2$	157
Figure 140: Variation in structural information obtained by mass spectrometric techniques	157
Figure 141: X-ray crystal structure for $[\text{Pd}(\text{MeCN})(\text{dmp}(\text{NHC}\{\text{Me}\})_2)][\text{OTf}]_2$, $R_1 = 10.72\%$	159
Figure 142: Displacement of benzonitrile and subsequent hydrolysis of acetonitrile	160
Figure 143: Ligand structural characteristics induced by palladium(II) coordination	160
Figure 144: X-ray structure for $[\text{Pd}(\text{OC}(\text{NH}_2)\text{Me})(\text{dmp}(\text{NHC}\{\text{Me}\})_2)]^+$, $R_1 = 4.85\%$	161
Figure 145: Theoretical binding modes for $[\text{Pd}(\text{C}_2\text{ONH}_5)(\text{dmp}(\text{NHC}\{\text{Me}\})_2)][\text{OTf}]_2$	162
Figure 146: ^1H NMR (d_6 -acetone) spectrum resulting from reactivity of $[\text{Pd}(\text{MeCN})(\text{dmp}(\text{NHC}\{\text{Me}\})_2)][\text{OTf}]_2$ with acetamide	163
Figure 147: ^1H NMR (d_6 -acetone) titration of $[\text{Pd}(\text{MeCN})(\text{dmp}(\text{NHC}\{\text{Me}\})_2)][\text{OTf}]_2$ with acetamide (■ = O-carboxamide, ● = imidol)	164
Figure 148: Amide-Imidol tautomerism of a platinum(II) triamine complex	165
Figure 149: % Conversion of acetonitrile into acetamide (cat. = 6 mol% $[\text{Pd}(\text{MeCN})(\text{dmp}(\text{NHC}\{\text{Me}\})_2)][\text{OTf}]_2$)	167
Figure 150: Internal vs. external nucleophilic attack of coordinated acetonitrile by water	168
Figure 151: Schematic for the formation of $[\text{PdCl}(\text{dmp}(\text{NHC}\{\text{Me}\})_2)][\text{OTf}]$ and $[\text{Pd}(\text{CN})(\text{dmp}(\text{NHC}\{\text{Me}\})_2)][\text{OTf}]$	168
Figure 152: X-Ray crystal structure for a co-crystallate of $[\text{Pd}(\text{CN})(\text{dmp}(\text{NHC}\{\text{Me}\})_2)][\text{OTf}]$ and $[\text{PdCl}(\text{dmp}(\text{NHC}\{\text{Me}\})_2)][\text{OTf}]$, $R_1 = 2.99\%$	170
Figure 153: Solid state characteristics of the $[\text{Pd}(\text{CN})(\text{dmp}(\text{NHC}\{\text{Me}\})_2)][\text{OTf}]$ and $[\text{Pd}(\text{CN})(\text{dmp}(\text{NHC}\{\text{Me}\})_2)][\text{OTf}]$ co-crystallate	171
Figure 154: Expansion of ^1H NMR (300 MHz, CD_2Cl_2) spectrum for $[\text{Rh}_2\text{Cl}_2(\text{COD})_2(\text{dmp}(\text{NHC}\{\text{Me}\})_2)]$	173
Figure 155: <i>Syn</i> and <i>anti</i> isomers of $[\text{Rh}_2\text{Cl}_2(\text{COD})_2(\text{dmp}(\text{NHC}\{\text{Me}\})_2)]$ and Crabtree's imidazol-2-ylidenes	173
Figure 156: Variable temperature ^1H NMR (d_6 -DMSO, 300-360 K) spectra of $[\text{Rh}_2\text{Cl}_2(\text{COD})_2(\text{dmp}(\text{NHC}\{\text{Me}\})_2)]$	175
Figure 157: Expansion of the $^{13}\text{C}\{^1\text{H}\}$ NMR (75 MHz, CD_2Cl_2) spectrum for $[\text{Rh}_2\text{Cl}_2(\text{COD})_2(\text{dmp}(\text{NHC}\{\text{Me}\})_2)]$	176
Figure 158: X-Ray crystal structure for $[\text{Rh}_2\text{Cl}_2(\text{COD})_2(\text{dmp}(\text{NHC}\{\text{Me}\})_2)]$, $R_1 = 8.49\%$	177
Figure 159: Possible formulations for the carbonylation product of $[\text{Rh}_2\text{Cl}_2(\text{CO})_4(\text{dmp}(\text{NHC}\{\text{Me}\})_2)]$	178
Figure 160: Expansion of the carbonyl region of the infrared spectrum (FT-ATR cm^{-1}) of the carbonylation product of $[\text{Rh}_2\text{Cl}_2(\text{COD})_2(\text{dmp}(\text{NHC}\{\text{Me}\})_2)]$	179
Figure 161: Selected quaternary carbons for $[\text{Rh}_2\text{Cl}_2(\text{CO})_4(\text{dmp}(\text{NHC}\{\text{Me}\})_2)]$ ($^{13}\text{C}\{^1\text{H}\}$ NMR, d_6 -DMSO)	181
Figure 162: Examples of Rh- C_{NHC} dicarbonyl complexes	181
Figure 163: Preparation of $[\text{Rh}_2(\mu\text{-CN})(\text{COD})_2(\text{dmp}(\text{NHC}\{\text{Me}\})_2)][\text{OTf}]$	182
Figure 164: Expansion of the ^1H NMR (300 MHz, CDCl_3) spectrum of $[\text{Rh}_2(\mu\text{-CN})(\text{COD})_2(\text{dmp}(\text{NHC}\{\text{Me}\})_2)][\text{OTf}]$	183
Figure 165: Expansion of the $^{13}\text{C}\{^1\text{H}\}$ NMR (75 MHz, CDCl_3) spectrum of	184
Figure 166: A $[(\text{C}_5\text{Me}_5\text{Rh}-\mu\text{-CH}_2)_2(\mu\text{-CN})_2][\text{PF}_6]$ dicationic rhodium tetrad with two bridging μ -cyano groups	184
Figure 167: X-ray crystal structure of the two isomers of $[\text{Rh}_2(\mu\text{-CN})(\text{COD})_2(\text{dmp}(\text{NHC}\{\text{Me}\})_2)][\text{OTf}]$ which appear in the solid state, $R_1 = 7.83\%$	186
Figure 168: Scheme for the formation of $[\text{Ir}(\text{COD})(\text{dmp}(\text{NHC}\{\text{Me}\})_2)][\text{OTf}]$	187
Figure 169: NOESY (mixing time of 600 ms) of $[\text{Ir}(\text{COD})(\text{dmp}(\text{NHC}\{\text{Me}\})_2)][\text{OTf}]$ demonstrating through space correlation of the bridging methylene protons	188
Figure 170: $[(\text{DEAM})\text{-IBY}]\text{Ir}(\text{COD})^+$ (A), a bisbenzimidazol-2-ylidene pincer complex	189
Figure 171: X-ray crystal structure for $[\text{Ir}(\text{COD})(\text{dmp}(\text{NHC}\{\text{Me}\})_2)][\text{OTf}]$ $R_1 = 4.9\%$, view from the pincer carbene face (counter-anion omitted for clarity)	190
Figure 172: X-ray crystal structure for $[\text{Ir}(\text{COD})(\text{dmp}(\text{NHC}\{\text{Me}\})_2)][\text{OTf}]$ $R_1 = 4.9\%$, view from the 1,5-cyclooctadiene occupied face (counter-anion omitted for clarity)	190
Figure 173: Intermolecular crystal packing interactions for $[\text{Ir}(\text{COD})(\text{dmp}(\text{NHC}\{\text{Me}\})_2)][\text{OTf}]$: (A) the unit cell, (B) viewed along the (-1 16 9) Miller plane	191
Figure 174: Cone angle exhibited by $\text{dmp}(\text{NHC}\{\text{Me}\})_2$ upon coordination to iridium(I)	191
Figure 175: Examples of the influence of mutually <i>trans</i> ligands and steric influence upon Ir- N_{py} bond distances	192

Figure 176: Preparation of $[\text{Ir}_2(\mu\text{-CN})(\text{COD})_2(\text{dmp}(\text{NHC}(\text{Me})_2))][\text{OTf}]$	194
Figure 177: NOESY (mixing time of 600 ms) of $[\text{Ir}_2(\mu\text{-CN})(\text{COD})_2(\text{dmp}(\text{NHC}(\text{Me})_2))][\text{OTf}]$ demonstrating through space correlation of the bridging methylene protons	195
Figure 178: Expansion of the quaternary carbon region of the $^{13}\text{C}\{^1\text{H}\}$ NMR spectrum (CDCl_3) for $[\text{Ir}_2(\mu\text{-CN})(\text{COD})_2(\text{dmp}(\text{NHC}(\text{Me})_2))][\text{OTf}]$	196
Figure 179: Overlay of the $^{13}\text{C}\{^1\text{H}\}$ NMR (CDCl_3) COD-CH regions for $[\text{Ir}_2(\mu\text{-CN})(\text{COD})_2(\text{dmp}(\text{NHC}(\text{Me})_2))][\text{OTf}]$ and $[\text{Rh}_2(\mu\text{-CN})(\text{COD})_2(\text{dmp}(\text{NHC}(\text{Me})_2))][\text{OTf}]$	196
Figure 180: Scheme for the reversible formation of $[\text{Ir}(\text{CO})(\text{COD})(\text{dmp}(\text{NHC}(\text{Me})_2))][\text{OTf}]$	197
Figure 181: Partial hydrolysis of $\text{SIPr}\cdot\text{HCl}$	199
Figure 182: Mechanism for the hydrolysis of the azole ring of benzimidazolium within $[(\text{dmp}(\text{NHC}(\text{Me})_2))_2][\text{OTf}]_2$	199
Figure 183: Transformations of formamide and <i>N,N</i> -dimethylformamide.....	200
Figure 184: Oxidative addition of a C-CN bond across $\text{Ni}(0)$	201
Figure 185: C-C bond cleavage of acetonitrile mediated by silver nitrate	201
Figure 186: Acetonitrile as a source for cyanide under ambient conditions	202
Figure 187: General schematic for the formation of $\text{H}_4\text{L}(\text{C}_2\text{H}_4)_2(\text{bzim})_2$	220
Figure 188: Mechanism for the aza-Michael addition.....	221
Figure 189: X-ray crystal structure for $\text{H}_4\text{L}(\text{C}_2\text{H}_4)_2(\text{bzim})_2$, $R_1 = 5.8\%$	223
Figure 190: Hydrogen bonding interactions and solid state packing characteristics of $\text{H}_4\text{L}(\text{C}_2\text{H}_4)_2(\text{bzim})_2$	224
Figure 191: Solvent occupation in the crystal packing of $\text{H}_4\text{L}(\text{C}_2\text{H}_4)_2(\text{bzim})_2$	225
Figure 192: HMBC ^{13}C - ^1H correlation experiment with $\text{H}_4\text{L}(\text{C}_2\text{H}_4)_2(\text{imid})_2$	226
Figure 193: Schematic for the formation of macrocyclic imidazolium and benzimidazolium salts.....	227
Figure 194: Crystal structure of $[\text{H}_4\text{L}(\text{C}_2\text{H}_4)_2(\text{bzim}_2\{\text{macro}\})][\text{Br}]_2$, $R_1=16.21\%$	228
Figure 195: Intramolecular angles of $[\text{H}_4\text{L}(\text{C}_2\text{H}_4)_2(\text{bzim}_2\{\text{macro}\})][\text{Br}]_2$ in the solid state.....	229
Figure 196: Overlay of the ^1H NMR spectra (d_6 -DMSO) for $[\text{H}_4\text{L}(\text{C}_2\text{H}_4)_2(\text{imid})_2]$ and $[\text{H}_4\text{L}(\text{C}_2\text{H}_4)_2(\text{imid}_2\{\text{macro}\})][\text{Br}]_2$	230
Figure 197: Two possible formulations for $[\text{H}_4\text{L}(\text{C}_2\text{H}_4)_2\text{HgBr}_2((\text{NHC})_2\{\text{macro}\})]_2$	233
Figure 198: Expansion of the $[\text{M}+\text{H}]^+$ (2313.2145 m/z) fragment of $[\text{H}_4\text{L}(\text{C}_2\text{H}_4)_2\text{HgBr}_2((\text{NHC})_2\{\text{macro}\})]_2$, ESI-MS	234
Figure 199: Expansion of the $[\text{M}-\text{Br}]^+$ (2233.2858 m/z) fragment of $[\text{H}_4\text{L}(\text{C}_2\text{H}_4)_2\text{HgBr}_2((\text{NHC})_2\{\text{macro}\})]_2$, ESI-MS	235
Figure 200: Expansion of the monomeric fragment ($\text{C}_{44}\text{H}_{36}\text{BrHgN}_{12}\text{O}_4^+$) of $[\text{H}_4\text{L}(\text{C}_2\text{H}_4)_2\text{HgBr}_2((\text{NHC})_2\{\text{macro}\})]_2$, ESI-MS	236
Figure 201: Examples of T-shaped geometry exhibited by mercury(II).....	238
Figure 202: Crystal structure of $[\text{H}_4\text{L}(\text{C}_2\text{H}_4)_2\text{Hg}((\text{NHC})_2\{\text{macro}\})][\text{HgBr}_4]$, $R_1 = 4.8\%$	238
Figure 203: Placement of the tetrabromomercurate anion within $[\text{H}_4\text{L}(\text{C}_2\text{H}_4)_2\text{Hg}((\text{NHC})_2\{\text{macro}\})][\text{HgBr}_4]$	240
Figure 204: Mercury(II) bisimidazol-2-ylidene substituted cyclophanes and pyridinophanes.....	242
Figure 205: ESI-MS of $[\text{H}_4\text{L}(\text{C}_2\text{H}_4)_2\text{PdX}((\text{NHC})_2\{\text{macro}\})]^+$ ($X=\text{Cl}$ or Br).....	243
Figure 206: Stacked overlay of the ^1H NMR (d_6 -DMSO) spectra for $[\text{H}_4\text{L}(\text{C}_2\text{H}_4)_2(\text{bzim}_2\{\text{macro}\})][\text{Br}]_2$, $[\text{H}_4\text{L}(\text{C}_2\text{H}_4)_2\text{HgBr}_2((\text{NHC})_2\{\text{macro}\})]_2$ and $[\text{H}_4\text{L}(\text{C}_2\text{H}_4)_2\text{PdCl}((\text{NHC})_2\{\text{macro}\})][\text{PF}_6]$	244
Figure 207: Stacked overlay of the Carbene, C=O and pyridyl quaternary ranges for $[\text{H}_4\text{L}(\text{C}_2\text{H}_4)_2(\text{bzim}_2\{\text{macro}\})][\text{Br}]_2$, $[\text{H}_4\text{L}(\text{C}_2\text{H}_4)_2\text{HgBr}_2((\text{NHC})_2\{\text{macro}\})]_2$ and $[\text{H}_4\text{L}(\text{C}_2\text{H}_4)_2\text{PdCl}((\text{NHC})_2\{\text{macro}\})][\text{PF}_6]$	245
Figure 208: Solution 0, $R_1 = 7.4\%$, GooF = 1.058.....	246
Figure 209: Proposed structure for a bimetallic complex of $[\text{H}_4\text{LPd}(\text{C}_2\text{H}_4)_2\text{PdCl}((\text{NHC})_2\{\text{macro}\})][\text{PF}_6]$	247
Figure 210: Simplified view of the macrocyclic cavity of $[\text{H}_4\text{L}(\text{C}_2\text{H}_4)_2\text{PdCl}((\text{NHC})_2\{\text{macro}\})][\text{PF}_6]$	248
Figure 211: X-ray crystal structure for $[\text{H}_4\text{L}(\text{C}_2\text{H}_4)_2\text{PdCl}((\text{NHC})_2\{\text{macro}\})][\text{PF}_6]$, views of the two coordination pockets, $R_1 = 6.5\%$, GooF = 1.054	249
Figure 212: Solid state packing characteristics of void filling solvent THF	251
Figure 213: Crystallographic solution 1, $R_1 = 6.5\%$, GooF = 1.054.....	252
Figure 214: Crystallographic solution 2, $R_1 = 6.5\%$, GooF = 1.052.....	253
Figure 215: Crystallographic solution 3, $R_1 = 6.5\%$, GooF = 1.046.....	253
Figure 216: Crystallographic solution 4	254
Figure 217: Crystallographic solution 5	254
Figure 218: Hydrosilylation of phenylacetylene leading to the formation of three major isomers.....	267
Figure 219: The Chalk-Harrod mechanism for hydrosilylation of terminal alkynes.....	268

Figure 220: The Crabtree-Ojima mechanism for hydrosilylation of terminal alkynes.....	269
Figure 221: Hydrosilylation of phenylacetylene using Karstedt's catalyst	270
Figure 222: Rhodium(I) and iridium(I) complexes of $(dmp(MHC\{Me\}_2))_2$	272
Figure 223: Example of a 1H NMR spectrum obtained from the hydrosilylation of phenylacetylene with triethoxysilane, cat. = $Rh_2Cl_2(COD)_2(dmp(MHC\{Me\}_2))_2$	274
Figure 224: Example of a 1H NMR spectrum obtained from the hydrosilylation of phenylacetylene with triethylsilane, cat. = $[Ir_2(\mu-CN)(COD)_2(dmp(MHC\{Me\}_2))][OTf]$	274
Figure 225: Example of a 1H NMR spectrum obtained from the hydrosilylation of phenylacetylene with triphenylsilane, cat. = $[Ir(COD)(dmp(MHC\{Me\}_2))][OTf]$	274
Figure 226: Catalytic activity of 3-Me ₂ and 3-Bu ₂ in the hydrosilylation of phenylacetylene with triethoxysilane.....	275
Figure 227: Characteristics of the hydrosilylation reaction between phenylacetylene and triethoxysilane, $Rh_2Cl_2(COD)_2(dmp(MHC\{Me\}_2))_2$ (1 mol%)	276
Figure 228: Characteristics of the hydrosilylation reaction between phenylacetylene and triethylsilane, $Rh_2Cl_2(COD)_2(dmp(MHC\{Me\}_2))_2$ (1 mol%)	277
Figure 229: Characteristics of the hydrosilylation reaction between phenylacetylene and triphenylsilane, $Rh_2Cl_2(COD)_2(dmp(MHC\{Me\}_2))_2$ (1 mol%)	278
Figure 230: Characteristics of the hydrosilylation reaction between phenylacetylene and triethoxysilane, $[Rh_2(\mu-CN)(COD)_2(dmp(MHC\{Me\}_2))][OTf]$ (1 mol%)	279
Figure 231: Characteristics of the hydrosilylation reaction between phenylacetylene and triethylsilane, $[Rh_2(\mu-CN)(COD)_2(dmp(MHC\{Me\}_2))][OTf]$ (1 mol%).....	280
Figure 232: Characteristics of the hydrosilylation reaction between phenylacetylene and triphenylsilane, $[Rh_2(\mu-CN)(COD)_2(dmp(MHC\{Me\}_2))][OTf]$ (1 mol%)	281
Figure 233: Characteristics of the hydrosilylation reaction between phenylacetylene and triethoxysilane, $[Ir_2(\mu-CN)(COD)_2(dmp(MHC\{Me\}_2))][OTf]$ (1 mol%).....	282
Figure 234: Characteristics of the hydrosilylation reaction between phenylacetylene and triethylsilane, $[Ir_2(\mu-CN)(COD)_2(dmp(MHC\{Me\}_2))][OTf]$ (1 mol%).....	283
Figure 235: Characteristics of the hydrosilylation reaction between phenylacetylene and triphenylsilane, $[Ir_2(\mu-CN)(COD)_2(dmp(MHC\{Me\}_2))][OTf]$ (1 mol%).....	284
Figure 236: Catalytic activity of a Rh(I) pincer MHC in the hydrosilylation of phenylacetylene with triethoxysilane.....	285
Figure 237: Characteristics of the hydrosilylation reaction between phenylacetylene and triethoxysilane, $[Ir(COD)(dmp(MHC\{Me\}_2))][OTf]$ (1 mol%).....	286
Figure 238: Characteristics of the hydrosilylation reaction between phenylacetylene and triethylsilane, $[Ir(COD)(dmp(MHC\{Me\}_2))][OTf]$ (1 mol%).....	287
Figure 239: Characteristics of the hydrosilylation reaction between phenylacetylene and triphenylsilane, $[Ir(COD)(dmp(MHC\{Me\}_2))][OTf]$	288
Figure 240: Typical catalysts for the Heck-Mizoroki reaction. The active species are $Pd^0(PPh_3)_2$ and $[Pd^0(PPh_3)_n(OAc)]$	291
Figure 241: General mechanism for the Heck-Mizoroki reaction in which Pd(0) and Pd(II) species are operative.....	292
Figure 242: Activity of palladium(II) mono-dentate versus pincer MHCs in Heck-Mizoroki reactions	293
Figure 243: The influence of ligand donor strength upon catalyst stability in the Heck-Mizoroki coupling reaction.....	294
Figure 244: Schematics for three Heck-Mizoroki reaction methodologies	298
Figure 245: Consumption profile for the Heck-Mizoroki coupling reaction between bromobenzene and styrene	300
Figure 246: Schematic for the determination of stilbenes against total aryl hydrogens	301
Figure 247: 1H NMR spectrum taken from Entry 3.....	305
Figure 248: Summary of the results from Heck reactions using macrocyclic palladium pincer $[H_4L(C_2H_4)_2PdBr((MHC)_2\{macro\})][PF_6]$	306
Figure 249: Structure of 4-APR resin and 2-aminopyridine on a silica support	308
Figure 250: Possible monomeric units for a palladium aggregate	309
Figure 251: The influence of palladium(II) coordination to amide infrared stretching frequencies	310
Figure 252: Proposed fragmentation pathway for $PdxAMPy$ from the base peak	311
Figure 253: ESI-MS of the palladium aggregate, featuring M+1 and M+2 ions.....	312
Figure 254: Rhenium cluster of $[Re_3(\mu-H)_3(CO)_{11}(MeCN)]$ and 2-amino-6-methyl pyridine	313
Figure 255: Relative activity of acyclic vs. macrocyclic pincer imidazol-2-ylidenes in the C-C coupling of 4-bromoacetophenone and ⁿ butyl acrylate (cat. 1×10^{-3} mol%, 24 hrs).....	315

Figure 256: A diagrammatic comparison between the coordination pockets of LMe_2 and $\text{dmp}(\text{NHC}(\text{Me})_2)$	316
Figure 257: Summary of the results from Heck reactions catalysed by palladium(II) pincer pyridine carboxamides	317
Figure 258: Reaction profile for $[\text{PdCl}(\text{LMe}_2\{\text{Me}\}_2)][\text{OTf}]$ in the C-C coupling reaction of bromobenzene and styrene.....	318

List of Tables

Table 1: Correlation of stericity and Bond Dissociation Energy with the Carbonyl stretching frequency (in CH ₂ Cl ₂) of a series of transition metal MHCs	31
Table 2: Selected bond lengths and angles for Rh(en)Cl(LMe ₂).....	78
Table 3: Selected bond lengths and angles for [RhCl ₂ (PPh ₃)(LMe ₂ {H} ₂)]Cl	82
Table 4: Selected bond lengths and angles in the complex [RhCl(LMe ₂) ₂].....	93
Table 5: Pertinent infrared stretching frequencies for methyl-pyridinium complexes.....	110
Table 6: Selected ¹³ C{ ¹ H} NMR (d ₆ -DMSO, ppm) chemical shifts for complexes bearing the L _{opy} {Me} ₂ ligand.....	111
Table 7: Results for the transfer hydrogenation of acetophenone by isopropanol in the presence of various metal complexes	127
Table 8: ¹ H and ¹³ C{ ¹ H} NMR (CDCl ₃) reference signals for acetophenone and 1-phenylethanol ...	150
Table 9: Selected bond lengths and angles for [dmp(bzim{Me}) ₂] ₂	155
Table 10: Selected NMR spectral characteristics for [(dien)Pt(DMU)][OTf] ₂ and [(dien)Pt(acetamide)][OTf] ₂	165
Table 11: Results for the conversion of acetonitrile into acetamide mediated by [Pd(MeCN)(dmp(MHC{Me}) ₂)] ₂ [OTf] ₂ (6 mol%) after 21 days	167
Table 12: Selected bond lengths and angles for [Rh ₂ Cl ₂ (COD) ₂ (dmp(MHC{Me}) ₂)].....	177
Table 13: Selected bond lengths and angles for [Ir(COD)(dmp(MHC{Me}) ₂)] ₂ [OTf].....	193
Table 14: ¹ H NMR (d ₆ -acetone, ppm) chemical shifts for acetamide, hexamethylbenzene and [Pd(MeCN)(dmp(MHC{Me}) ₂)] ₂ [OTf] ₂	209
Table 15: Selected bond lengths and angles for [H ₄ L(C ₂ H ₄) ₂ Hg((MHC) ₂ {macro})][HgBr ₄].....	239
Table 16: Tabulated intramolecular characteristics of [H ₄ L(C ₂ H ₄) ₂ PdCl((MHC) ₂ {macro})][PF ₆].....	250
Table 17: ¹ H NMR signals pertaining to the alkenyl isomers of several vinylsilanes	273
Table 18: ¹ H NMR signals pertaining to the specific reactants in hydrosilylation reactions	273
Table 19: Summarised results for the hydrosilylation of phenylacetylene.....	289
Table 20: Chemical shifts corresponding to the alkenyl protons of styrene and stilbenes in the C-C coupling reaction of bromobenzene with styrene	296
Table 21: Chemical shifts corresponding to the alkenyl protons of ⁿ butyl acrylate and ⁿ butyl cinnamates in the C-C coupling reaction of bromobenzene with ⁿ butyl acrylate.....	296
Table 22: Summarised reaction conditions for methods 1-3	297
Table 23: Estimated experimental errors.....	302
Table 24: Heck-Mizoroki reaction with [PdBr(dmp(MHC{Me}) ₂)] ₂ [OTf] and PdCl ₂	303
Table 25: Summary of the results from Heck reactions using acyclic palladium pincer bisbenzimidazol-2-ylidenes	304
Table 26: Summary of the results from reference Heck reactions catalysed by palladium(II) amines	313
Table 27: Summary of the results from reference Heck reactions catalysed by palladium(II) MHCs	314

List of Equations

Equation 1:	BDE = $-\Delta H/n(\text{bonds formed})$ kcal/mol.....	28
Equation 2:	Association of two electron donor ligands to $[\text{Cp}^*\text{RuCl}]_4$	28
Equation 3:	Metal Carbonyl resonance forms.....	31
Equation 4:	Formation of $\text{Ni}(\text{CO})_3\text{L}$	31

Abbreviations

1D	=	One dimensional
2D	=	Two dimensional
Ad	=	Adamantyl
ADPS	=	Anisotropic Displacement Parameters
BASF	=	Batch scale factors
BDE	=	Bond Dissociation Energy
BINAP	=	2,2'-Bis(diphenylphosphino)-1,1'-binaphthyl
bpy	=	Bipyridine
bpydb	=	Bipyridine diboronic acid
bzim{Me}	=	<i>N</i> -methylbenzimidazole
Calc.	=	Calculated
CCDB	=	Cambridge Crystallographic Database
CD	=	Circular dichroism
COD	=	1,5-Cyclooctadiene
COSY	=	Homonuclear correlation spectroscopy
Cp	=	Cyclopentadiene
Cp*	=	Pentamethylcyclopentadienyl
Cy	=	Cyclohexyl
cyclen	=	1,4,7,10-tetraazacyclododecane
d	=	Doublet
DABCO	=	1,4-diazabicyclo[2.2.2]octane
dba	=	Dibenzylacetone
DBU	=	1,8-Diazabicyclo[5.4.0]undec-7-ene
DCM	=	Dichloromethane
DEAM	=	Dihydro-9,10-ethanoanthracene
DELU	=	A restraint to bring the magnitude of the ADPs of neighbouring anisotropic atoms into closer agreement
DEPT 135	=	Distortionless Enhancement by Polarisation Transfer, 135° pulse angle
dft	=	Density Functional Theory
dien	=	Diethylenetriamine
DMAC	=	<i>N,N</i> -Dimethylacetamide
DMAP	=	4-Dimethylaminopyridine
DMF	=	<i>N,N</i> -Dimethylformamide
dmp	=	2,6-Dimethylpyridine
DMSO	=	Dimethylsulfoxide

DMU	=	1,1-Dimethylurea
dvds	=	1,3-Tetramethyl-divinyl-disiloxane
E.A.	=	Elemental Analysis
EADP	=	Equal Anisotropic Displacement Parameter
ee	=	Enantiomeric Excess
ESI-MS	=	Electrospray ionisation mass spectrum
FAB-MS	=	Fast Atom Bombardment mass spectrum
HMBC	=	Heteronuclear Multiple Bond Correlation
HSQC	=	Heteronuclear Single Quantum Coherence
IBY	=	Isopropylbenzimidazolidine-2-ylidene)
IPA	=	Isopropyl alcohol
IR	=	Infrared
ISOR	=	A restraint to make an anisotropic atom more isotropic-like
m	=	Multiplet (NMR) / Medium (IR)
macro	=	Macrocyclic
Mes	=	Mesityl
MHMDS	=	Alkali metal (Li or K) Hexamethyldisilazane
MIDA	=	<i>N</i> -methyliminodiacetic acid
MS	=	Mass Spectrometry
MHC	=	<i>N</i> -Heterocyclic Carbene
NMR	=	Nuclear Magnetic Resonance
OAc	=	Acetate
ORTEP	=	Oak Ridge Thermal Ellipsoid Plot
PCy ₃	=	Tricyclohexylphosphine
PPh ₃	=	Triphenylphosphine
Pr	=	Propyl
q	=	Quaternary
s	=	Singlet
s.d.	=	Standard deviation
SIMU	=	Similar U _{ij}
S/N	=	Signal to noise ratio
t	=	Triplet
terpy	=	Terpyridine
THF	=	Tetrahydrofuran
TMS	=	Tetramethylsilane
TOF	=	Turnover frequency
TON	=	Turnover numbers
TOPSPIN	=	TopSpin NMR software package developed by Bruker
d ₄ -TSPA	=	3-(trimethylsilyl) 3,3,2,2-tetradeuteropropionic acid Na salt
VT-NMR	=	Variable Temperature Nuclear Magnetic Resonance

Xphos = 2-Dicyclohexylphosphino-2',4',6'-triisopropylbiphenyl
zgpg = Pulse program with a continuous pulse decoupling mode